Phys. Status Solidi A **209**, No. 5, 854–858 (2012) / **DOI** 10.1002/pssa.201100793

physica status solidi pss a
www.pss-a.com
applications and materials science

Selective dissolution in AlFeNb alloys

Stefanie Drensler[1], Cezarina Cela Mardare[1], Srdjan Milenkovic[2], and Achim Walter Hassel[*,1]

[1] Institute for Chemical Technology of Inorganic Materials, Johannes Kepler University, Altenberger Str. 69, 4040 Linz, Austria
[2] IMDEA Materials, Parque Científico de la Universidad Carlos III de Madrid, Avda. del mar Mediterráneo 22, 28918 Leganés, Spain

Received 14 November 2011, revised 1 March 2012, accepted 27 March 2012
Published online 25 April 2012

Keywords intermetallic phases, iron aluminides, niobium, selective dealloying

[*] Corresponding author: e-mail achimwalter.hassel@jku.at, Phone: +43 732 2468 8700, Fax: +43 732 2468 8905

Three different AlFeNb alloys of various compositions were prepared by arc melting. X-ray diffraction (XRD) investigation of the melted samples proved the presence of two phases identified as a bcc α(Fe,Al) solid solution and a hexagonal C14 $(Fe,Al)_2Nb$ Laves phase. Subsequent electrochemical treatment allowed for a selective dealloying of the α(Fe,Al) or respective FeAl phase and resulted in releasing differently microstructured surfaces. These structures ranged from regular lamellar structures towards branched, fibrous structures. Scanning electron microscope (SEM) characterisation along with a local energy dispersive X-ray spectroscopic (EDX) analysis of the samples and atomic absorption spectrometry (AAS) analysis of the electrolyte revealed a preferential Fe dissolution and the passive nature of the Nb. The results demonstrate that the phases present in the alloys strongly depend on the production and heat treatment history of the sample.

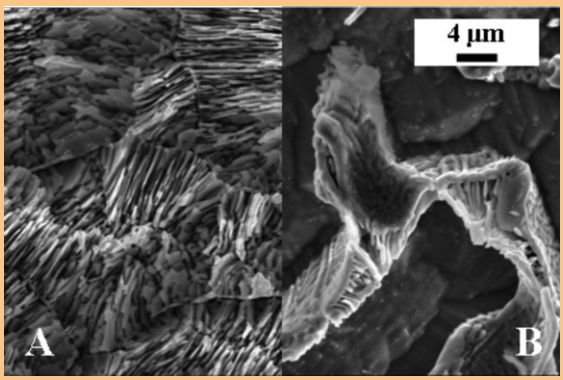

SEM micrograph of (A) Fe-15Al-10Nb and (B) Fe-26Al-4Nb after anodisation in 0.4 M borate buffer.

1 Introduction Development of iron aluminides, based on Fe_3Al, for applications in high temperature environments is an important area of research, as these materials possess unique properties such as, high strength to weight ratio, good wear resistance, excellent oxidation, and sulphidation resistance [1–4]. This oxidation and sulphidation resistance can be attributed to the formation of an external, protective alumina scale [5–9], which is more stable under these environmental conditions. In addition, they can be produced and manufactured using standard equipment, their cost is lower than that of stainless steels and also their application would avoid the use of strategic elements like Ni. Therefore, they may be considered as an alternative to high-alloyed steels or Ni-based superalloys for applications at elevated and high temperatures in corrosive environments. However, insufficient strength and inadequate creep resistance at high temperatures has been for long time the major obstacle which prevented the use of Fe–Al-based alloys for such applications [10–13].

In order to improve strength at high temperatures numerous investigations have been performed, many of them focussing on strengthening by incoherent precipitates of second phases [14]. An alternative method of material reinforcement is the incorporation of the second phase through directional solidification (DS) of eutectic alloys. The main advantage that DS eutectics have over other two-phase materials is a natural chemical and mechanical compatibility between the reinforcement and the matrix, which is an extremely important feature for high-temperature applications in hostile environments over extended periods of time. Furthermore, it is possible to tune the properties of the material by the processing conditions [15, 16]. DS of eutectics allows forming lamellar or fibrous structures in which the more expensive elements are the minor phases. This is in particular the case for materials such as NiAl-*X* where *X* can be W, Mo or Re [17]. Those fibrous structures may carry a significant mechanical load and in this way they are promising candidates to improve materials properties

among others the before said Fe–Al-base alloys. Quantitative measurements of the possible yield strength were carried out for electrochemically released Re nanowires [18] and methods like atomic force microscopy (AFM), NEMS (nano-electro mechanical systems) have been quantitatively applied to W nanowires [19]. A recent investigation on the Fe-26Al-9.5Nb alloy indicated that it possesses better high temperature strength and creep properties than binary Fe-26Al, and creep properties comparable to P92, a state-of-the-art steel for steam turbine applications [20]. An investigation like the before mentioned mechanical studies on single nanowires requires a selective dissolution of the forming phases. It is therefore of significant importance to understand the effect of the different alloying elements on the chemical and electrochemical stability of the phases. This aspect is addressed in this work for three different Nb containing FeAl alloys.

2 Experimental procedures

2.1 Sample preparation Two pre-alloys of nominal compositions Fe-15Al-10Nb and Fe-26Al-9.6Nb (all compositions in at.% except where noted) were prepared from high purity Al (99.9999 wt.%), Nb (99.9 wt.%) and Fe (99.9 wt.%) by induction melting under inert Ar atmosphere and drop casting into a cylindrical copper mould. A third pre-alloy of nominal composition Fe-26Al-4Nb was produced by levitation melting using the same high purity metals.

The pre-alloys were melted under Ar atmosphere using a home-made arc melting furnace. The base pressure was 40 Pa and the chamber was three times evacuated and filled with Ar (99.998% purity) before the melting process. Ar was introduced until atmospheric pressure was reached and a Ti getter was melted several times in order to absorb the residual oxygen from the chamber, with the chamber being pumped and flushed with Ar in between. Without opening the chamber to atmosphere, the pre-alloys were melted by creating an arc discharge using a high voltage between a W tip and the sample. The arc was then maintained until the alloys were in liquid phase. The melting point of Fe-26Al-*x*Nb alloys with low Nb content is in the range of 1500 °C for $x = 0$ to approximately 1350 °C for $x = 10$ [21]. The temperature of the arc can be different for different furnaces. In the present case, in order to ensure that the melting points of the alloys were reached and to have an indication about the temperature of the arc, pure Nb was also melted (melting point 2468 °C). Therefore, it can be concluded that the temperature of the arc was high enough to completely melt the Fe–Al–Nb alloys.

The compositions of these Fe-based alloys are shown in Table 1. All samples were ground with SiC paper up to 4000 grit, polished with 3 μm-diamond slurry, rinsed and ultrasonicated in ethanol and dried to remove residues from the surface preparation processes. Subsequent etching was performed to remove native oxides using a mixture of 25 mL H_2SO_4 (95–97%, Merck), 10 mL HNO_3 (65%, VWR), 20 mL HF (40%, Merck) and 20 mL of deionised water with immersion times of 15 s.

Table 1 Overall composition of the prepared samples.

sample	composition (at.%)
S1	75.0Fe-15.0Al-10.0Nb
S2	64.4Fe-26.0Al-9.6Nb
S3	70.0Fe-26.0Al-4.0Nb

2.2 Solutions and electrochemical procedures In order to characterise the surface properties a sequence of cyclic voltammograms with a stepwise increase of 1 V versus standard hydrogen electrode (SHE) up to a potential of 8 V (SHE) with a step rate 50 mV/s in a 0.4 M borate buffer solution (pH = 8.0) was utilised to anodise the surface. The buffer solution was prepared using sodium tetraborate decahydrate (per analysis, Merck) and boric acid (per analysis, Merck). For all electrochemical measurements an Impedance/Gain-Phase Analyzer (Solartron SI 1260) was coupled with an Electrochemical Interface (Solartron 1287).

2.2 Analytical methods The microstructure of the samples was furthermore analysed using a field emission scanning electron microscope (SEM, Zeiss LEO 1540XB) equipped with an energy dispersive X-ray spectroscope (EDX, Oxford Instruments). Quantification of dissolved metals in used buffer solutions was performed with an AAS (Hitachi Z-8230 Polarized Zeeman Atomic Absorption Spectrophotometer). X-ray diffraction (XRD, Philips Pro X'pert) with a CuK_α radiation and working in Bragg–Brentano geometry was used for the crystalline phase analysis. Due to the relatively small sample sizes (approximately 1–1.5 cm length and 0.5–0.7 mm width) a mono-capillary having 500 μm diameter was used for confining the X-ray beam.

3 Results and discussion

3.1 Microstructure of arc-melted samples Initial surface analysis of the samples proved significantly differing microstructures dependent on their Nb content. Two phases could be observed in the SEM images, a light grey one and a dark one, as shown as an example for Fe-26Al-9.6Nb in Fig. 1. Cellular structures revealing a fibrous morphology were obtained for samples with an Nb content of 9.6 and 10 at.%. In contrast to this the Fe-26Al-4Nb sample exhibits a typical structure consisting of primary dendrites (large dark areas) which are enclosed by an eutectic mixture (mixture of light grey/dark regions).

The EDX analysis performed on these different phases is shown in Table 2. The dark regions are mainly composed of Fe and Al, with a low Nb content, whereas the brighter regions are enriched in Nb (>20 at.%).

Corroborating the Fe–Al–Nb phase diagram (Fig. 2), the SEM images (Fig. 1) and the EDX results (Table 2) with the report from Palm [22], it is suggested that the dark phase should be α(Fe,Al) or FeAl, and the light grey $(Fe,Al)_2Nb$ Laves phase.

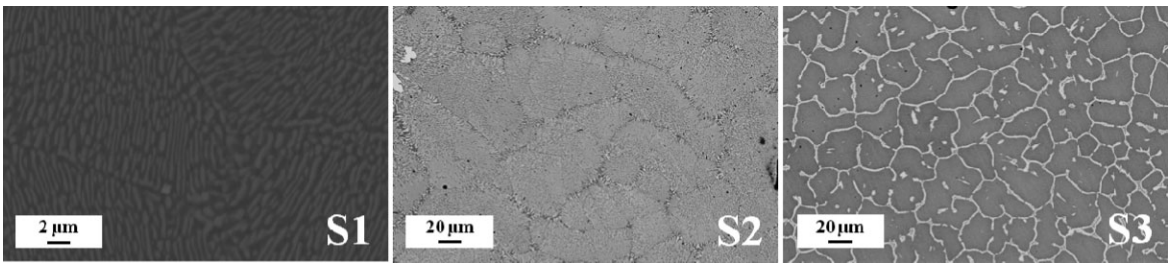

Figure 1 SEM micrographs of the re-melted samples possessing two present intermetallic phases. A minimum number of primary dendrites of the Laves phase is present in both S1 and S2 as visible in the upper left corner of S2.

Both FeAl and Fe_2Nb intermetallic compounds are not line compounds and exhibit a large homogeneity range. According to the binary Al–Fe phase diagram, the ordered intermetallic compound FeAl with B2 structure exists in the range between 23 and 54 at.% Al [23]. On the other hand, for the binary Fe–Nb system, existing data for the composition of the Laves phase are quite controversial. It has been reported that the Fe-rich boundary of the Laves phase may be at Nb contents as low as 22 at.% [24] or as high as 32 at.% Nb [25]. According to the more recent studies on the Fe–Al–Nb ternary system [22], the Fe-rich phase boundary of the Laves phase does not shift markedly with temperature, *i.e.* the Nb content is about 27 at.%. Slightly lower values obtained in the present work are within error of the technique used.

Figure 3 shows a comparison of the XRD diffractograms for the three alloys after the arc melting process, as well as the powder diffraction patterns for FeAl, α(Fe,Al) and Fe_3Al. For samples S1 and S3, the diffraction peaks were attributed to the bcc α(Fe,Al) solid solution having an A2 distorted structure (space group Im-3m, W-type, Pearson symbol cI2) and to the hexagonal C14 $(Fe,Al)_2Nb$ Laves phases (space group P63/mmc, $MgZn_2$-type, hP12) [22, 26]. Sample S2 has an additional peak at $2\theta = 30.7°$, which is an indication that the FeAl phase having ordered B2 structure (Pm-3m, CsCl-type, cP2) is present. Palm also found this phase for Fe-25Al-5Nb alloys after heat treatment at 1150 °C followed by quenching. Considering the phase diagram, where the FeAl stability range starts from 23 to 34 at.% Al, it was assumed that the Fe-25Al-5Nb alloy consists of α(Fe,Al) which was transformed to FeAl during cooling [23]. The presence for sample S2 of only one additional peak which might be attributed to the ordered FeAl phase, corroborated with the overlapping of the other two peaks (2θ approximately 44° and 81°) belonging to both FeAl and α(Fe,Al) phases, as indicated by the powder diffraction patterns, makes it nevertheless difficult to draw a clear conclusion upon the presence of a complete or partial ordering of the Fe–Al matrix during cooling. Another aspect to be considered is that the peak attributed to FeAl phase was found for the sample S2, but not for S3 which has a composition closer to the one used by Palm.

Table 2 EDX analysis of the alloys in the regions with different structures.

sample	composition (at.%)					
	dark regions			light grey regions		
	Fe	Al	Nb	Fe	Al	Nb
S1	80.1	18.8	1.1	65.0	12.2	22.8
S2	70.1	28.2	1.7	53.9	20.5	25.6
S3	70.0	27.1	2.9	53.7	20.7	25.6

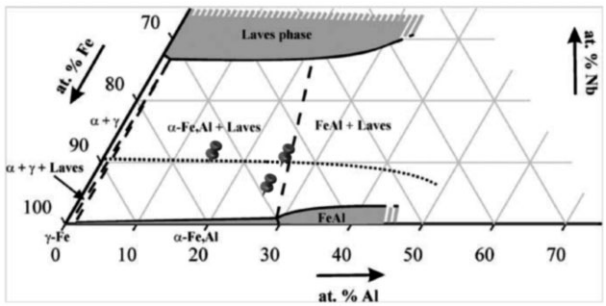

Figure 2 Partial isothermal cross-section of the FeAlNb system in the Fe-rich corner at 1000 °C [20]. The three pins mark the overall composition of the investigated alloys within the phase diagram.

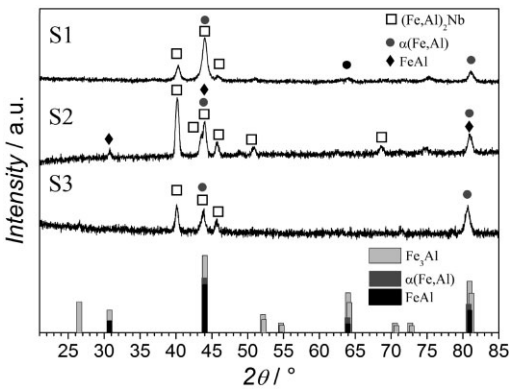

Figure 3 X-ray diffractograms of the alloys obtained by arc melting showing the presence of an FeAl phase and $(Fe,Al)_2Nb$ Laves phase, together with the powder diffraction patterns for FeAl, α(Fe,Al) and Fe_3Al.

The reason for the presence of different phases for the same composition can be due to the preparation methods. For an alloy with similar composition (Fe-26Al-9.5Nb) to S2, but obtained by DS, Milenkovic and Palm [20] found by electron backscatter diffraction (EBSD) the Fe_3Al phase together with the $(Fe,Al)_2Nb$ Laves phase. The authors explained this based on a low solid solubility of Nb in α(Fe,Al) leading to a similar transformation temperature for Fe_3Al/FeAl as in the binary alloys (550 °C). Here, it should be mentioned that in spite of very similar positions of the diffraction peaks for the Fe_3Al, α(Fe,Al) and FeAl phase, the presence of Fe_3Al was not considered in the present work. The reason is that the arc melting process involves very high melting temperatures (>2468 °C) followed by a rapid cooling more similar to a quenching process as opposed to a slow cooling process such as DS. The fast cooling is dictated by the water cooled copper mould in which the alloy is placed for being melted. This should inhibit the formation of the low temperature Fe_3Al, as a 'freezing' of the high temperature phases is expected for very high cooling rates. As already mentioned, Palm [22] found out that for an alloy (Fe-25Al-5Nb) with a composition similar to S3, but obtained by levitation melting and casting that there is a change from α(Fe,Al) to FeAl which depends on the heat treatment temperature of the quenched alloys.

3.2 Selective dealloying After initial surface analysis of the melted alloys, the electrochemical behaviour of the samples was investigated. Therefore, the samples were anodised in a 0.4 M borate buffer solution through a sequence of cyclic voltammograms. The SEM micrographs, shown in Fig. 4, depict in contrast to the melted samples from Fig. 1 solely a light grey phase having a well-arranged fibrous to lamellar structure for both samples S1 and S2. In accordance to this a similar behaviour was found for sample S3, obtaining only a small overall Nb content showing a strongly branched fibrous morphology seemingly emerging from the interdendritic areas. A supplementary EDX analysis on the electrochemically treated surface confirmed the absence of the dark α(Fe,Al) and respective FeAl phase for S1 and S2, confirming the obtained fibrous to lamellar structures to be the $(Fe,Al)_2Nb$ Laves phase. The light grey phases of sample S3 exhibit the same $(Fe,Al)_2Nb$ phase protruding from the enclosing Nb-depleted phase. Thus, through the combination of the analytical methods, a selective dealloying for all samples could be proven resulting from dissolution of the phase with low Nb content.

This phase selective dissolution is attributed to the difference in the overall valve metal content of the two phases which results in major differences in their passive behaviour. Al and Nb are both valve metals, that are materials which form an oxide upon anodic polarisation that is not reduced back to the metal in the reverse scan [27]. The α(Fe,Al) or respective FeAl phase only exhibits contents of valve metals varying from 19.9 to almost 30 at.%. Besides this fact, the overall content of valve metals is too low to reach the so called percolation threshold. Similar assump-

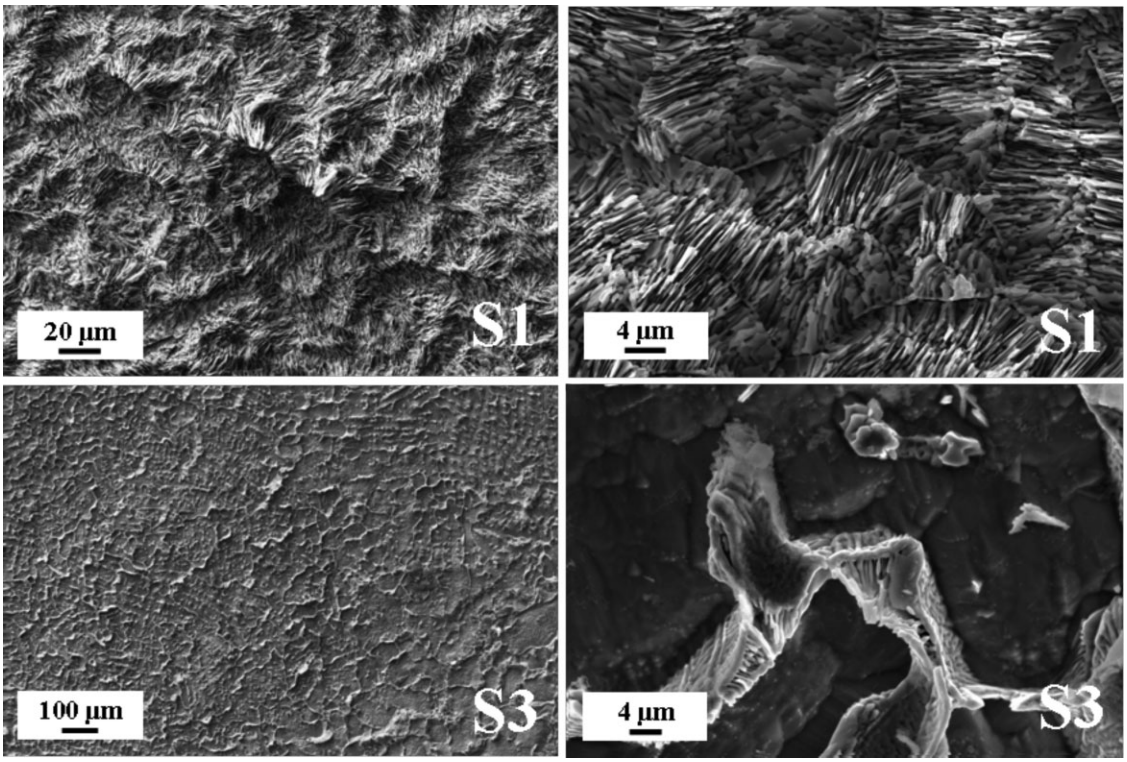

Figure 4 SEM micrographs showing the morphology after anodisation in 0.4 M borate buffer. The upper micrographs show aligned lamellar to fibrous structures of the light grey $(Fe,Al)_2Nb$ phase of sample S1. The lower micrographs depict the obtained branched structures protruding from the dissolved α(Fe,Al) phase of sample S3.

tions have already been made by Olsson and Landolt [28] for stainless steels. According to the percolation theory a specific amount of the minor element Cr in the major Fe-matrix is necessary to form a continuous network of atoms. The gap in between neighbouring Cr atoms can then be bridged by a oxide chain resulting in an overall surface passivation as reported by Newman et al. [29]. Transferring that aspect to the system studied here the valve metal content is too low to ensure an overall passivation of the surface which leads to the observed dissolution. Dissolution of both, Fe and Al could be confirmed by the AAS analysis of the buffer solutions used.

The composition of preserved Laves phase structures reach a valve metal content up to more than 40 at.%. Furthermore, this Laves phase has a relatively high content of Nb which is showing an even stronger passive behaviour as compared to Al [30]. The combination of these properties explains why a protective passive layer forms on this phase hindering further dissolution.

4 Summary Three Fe-based alloys with varying amounts of Al and Nb were produced by arc melting. Investigation of the melted samples proved the presence of two phases identified as a bcc α(Fe,Al) solid solution having a A2 distorted structure (space group Im-3m, W-type, Pearson symbol cI2) and a hexagonal C14 $(Fe,Al)_2Nb$ Laves phase (space group $P6_3/mmc$, $MgZn_2$-type, hP12). A clear conclusion upon the presence of an FeAl phase cannot be drawn due to a peak which might be attributed to both FeAl and α(Fe,Al). Through a subsequent electrochemical treatment of the samples a selective dealloying of the α(Fe,Al) or respective FeAl phase could be achieved releasing different microstructured surfaces. Depending on the composition different structures ranging from regular lamellar to fibrous structures towards branched, fibrous structures could be obtained. The results demonstrate that the phases present in the alloys strongly depend on the production and heat treatment history of the sample, and detailed investigation for arc melted alloys being the topic of a further publication.

Acknowledgements The authors are indebted to G. Knör and H. Peirlberger from the Institute for Inorganic Chemistry at the Johannes Kepler University Linz, Austria for making the arc melting furnace available.

References

[1] W. J. Quadakkers, D. Naumenko, and E. Wessel, Oxid. Met. **61**, 17 (2004).
[2] H. Al-Badairy and G. J. Tatlock, Oxid. Met. **53**, 157 (2000).
[3] I. G. Wright, R. Peraldi, and B. A. Bint, Mater. Sci. Forum **461–464**, 579 (2004).
[4] S. J. Taniguchi and A. Andoh, Oxid. Met. **52**, 1 (1999).
[5] N. S. Stoloff, Int. Met. Rev. **29**, 123 (1984).
[6] C. G. McKamey, J. H. DeVan, P. F. Tortorelli, and V. K. Sikka, J. Mater. Res. **6**, 1779 (1991).
[7] S. C. Deevi and V. K. Sikka, Intermetallics **4**, 357 (1996).
[8] C. T. Liu, J. O. Stiegler, and F. H. Froes, Ordered Intermetallics, Metals Handbook, 10th ed., Vol. 2 (ASM, Metals Park, USA, 1990), p. 913.
[9] C. T. Liu and K. S. Kumar, J. Met. **45**, 38 (1993).
[10] A. Bahadur, Mater. Sci. Technol. **19**, 1627 (2003).
[11] D. H. Sastry and R. S. Sundar, in: Int. Symp. on Nickel and Iron Aluminides: Processing, Properties, and Applications, edited by S. C. Deevi, P. J. Maziasz, V. K. Sikka, and R. W. Cahn (ASM Int., Materials Park, 1997), p. 123.
[12] D. G. Morris and M. A. Morris, Mater. Sci. Eng. A **239**, 23 (1997).
[13] D. G. Morris, Intermetallics **6**, 753 (1998).
[14] M. Palm, Intermetallics **13**, 1286 (2005).
[15] S. Milenkovic, A. W. Hassel, and A. Schneider, Nano Lett. **6**, 794 (2006).
[16] S. Milenkovic and A. W. Hassel, Phys. Status Solidi A **206**, 455 (2009).
[17] A. W. Hassel, B. Bello-Rodriguez, A. J. Smith, Y. Chen, and S. Milenkovic, Phys. Status Solidi B **247**, 2380 (2010).
[18] L. Philippe, I. Peyrot, J. Michler, A. W. Hassel, and S. Milenkovic, Appl. Phys. Lett. **91**, 111919 (2007).
[19] V. Cimalla, C. C. Röhlig, J. Pezoldt, M. Niebelschütz, O. Ambacher, K. Brückner, M. Hein, J. Weber, S. Milenkovic, A. J. Smith, and A. W. Hassel, J. Nanomater. **2008**, 638947 (2008).
[20] S. Milenkovic and M. Palm, Intermetallics **16**, 1212 (2008).
[21] O. Prymak and F. Stein, Intermetallics **18**, 1322 (2010).
[22] M. Palm, J. Alloys Compd. **475**, 173 (2009).
[23] O. Kubaschewski, Iron – Binary Phase Diagrams (Springer-Verlag Stahleisen, Berlin/Düsseldorf, 1982), p. 70.
[24] J. M. Z. Bejarano, S. Gama, C. A. Ribeiro, G. Effenberg, and C. Santos, Z. Metallkd. **84**, 160 (1993).
[25] H. J. Goldschmidt, J. Iron Steel Inst. **194**, 169 (1960).
[26] J. M. Park, K. B. Kim, W. T. Kim, M. H. Lee, J. Eckert, and D. H. Kim, Intermetallics **16**, 642 (2008).
[27] A. W. Hassel and D. Diesing, Thin Solid Films **414**, 296 (2002).
[28] C.-O. A. Olsson and D. Landolt, Electrochim. Acta **48**, 1093 (2003).
[29] R. C. Newman, F. T. Meng, and K. Sieradzki, Corros. Sci. **28**, 523 (1988).
[30] M. Pourbaix, Atlas of Electrochemical Equilibria in Aqueous Solutions (Pergamon Press, Headington Hill, Oxford, 1966).

